NetCorr: A Resection-Induced Network Perturbation Framework for Predicting Seizure Freedom in Drug-Resistant Epilepsy

Tonmoy Monsoor[1], Sotaro Kanai[2], Lina Zhang[1], Atsuro Daida[2], Prateik Sinha[1], Hiroki Nariai[2], and Vwani Roychowdhury[1]

[1] Department of Electrical and Computer Engineering, UCLA
[2] Department of Neurology, UCLA
vwani@g.ucla.edu

Abstract. Drug-resistant epilepsy (DRE) is often treated with resective surgery, yet a central clinical challenge remains: given a planned (or completed) resection, what is the likelihood the patient will achieve seizure freedom? Answering this is difficult because the optimal surgical target—the epileptogenic zone (EZ), the brain tissue that generates seizures—is latent and must be inferred from biomarkers derived from intracranial EEG (iEEG). Biomarkers at both channel and network level have been developed and evaluated as independent sources of data stream and thus have shown limited promise in predicting surgical outcomes. We hypothesize that the channel and network level biomarkers are mechanistically connected, and introduce NetCorr, a platform that makes use of this underlying correlation to better predict seizure freedom. Towards this end, we first introduce a regression framework that predicts a channel's smoothed high-frequency-oscillation with spike (spkHFO) rate from its participation properties in a ripple-band synchronization network, quantifying network-spkHFO coupling via R^2. Secondly, we model resection as a perturbation of the preserved channel coupling scores and construct a 2-dimensional patient signature that summarizes resection-induced shifts in coupling statistics. In a multi-institutional retrospective cohort of 159 pediatric-onset focal DRE patients, this 2-dimensional signature predicts post-surgical outcome with a cross-validated mean $F1$ score of 95%, significantly outperforming ratio-based baselines using SOZ resection ($F1 = 78\%$) and spkHFO resection ($F1 = 79\%$).

Keywords: Drug resistant epilepsy · Seizure freedom prediction · Synchronization network · HFO with spikes · Network perturbation

1 Introduction and Prior Work

Epilepsy affects tens of millions of people worldwide and is associated with substantial morbidity, mortality, and socioeconomic burden [21, 7, 3]. A clinically important subset develops *drug-resistant epilepsy* (DRE), typically defined as failure of two appropriate and tolerated antiseizure medication regimens [11].

For patients with focal DRE, resective surgery often offers the best chance of seizure freedom [19, 6, 10]. The central clinical problem is therefore predictive: *given a planned (or performed) resection, what is the probability that the patient will become seizure-free?* This question is difficult because the intended surgical target—the epileptogenic zone (EZ), i.e., the critical brain region responsible for seizure generation—is a latent construct that cannot be directly observed in vivo [14, 5]. In practice, the EZ must be inferred from imperfect proxies, and surgical failure may reflect not only imperfect targeting but also incomplete sampling of the epileptogenic network by implanted electrodes [16, 10].

A common clinical strategy is to use intracranial EEG (iEEG), guided by presurgical imaging and other evaluations, to record seizures and identify the seizure onset zone (SOZ) as a practical approximation to the EZ [14, 5]. However, ictal activity occupies only a small fraction of the total recording, and SOZ-guided resection does not consistently yield seizure freedom across patients [6, 10]. This has motivated growing interest in *interictal* features or biomarkers that can leverage the much larger amount of non-seizure data (interictal) to better approximate EZ-related tissue and improve surgical decision-making.

Existing interictal approaches span multiple spatial scales. At the *channel level*, spikes, high-frequency oscillations (HFOs), and their refinements (including epileptogenic HFOs and spike-associated HFO(spkHFO)) capture local pathological activity and have shown value for EZ localization and postsurgical outcome prediction, but remain susceptible to physiological confounds and detection variability [9, 18, 24, 15]. At the *network level*, interictal connectivity and dynamical approaches (e.g., Source–Sink and Neural Fragility) model epilepsy as a distributed circuit disorder and can reveal epileptogenic structure not captured by local pathological event rates alone [8, 12, 16, 1]. However, *these two lines of work – network and channel levels – have evolved separately, and a methodology for using these findings jointly to inform seizure freedom outcome has not been developed.* To address this missing link we first ask the following question in this paper: (1) *How well can the channel-level pathological event temporal dynamics be predicted by network dynamics?*

As described in Sections 2.3 and 2.4, we introduce a *synchronization network–spkHFO coupling framework* (NetCorr) for processing interictal iEEG. In this framework we first construct ripple-band (80–250 Hz) directed synchronization networks based on phase-amplitude coupling in the frequency domain. For channel-level biomarkers, we identify spkHFOs using PyHFO [4]. We then fit per-channel regression models predicting smoothed spkHFO rates using network-level features of the channel (in-degree, out-degree, eigenvector centrality), yielding channel-wise coupling or correlation scores (R^2). A high R^2 would imply that the spkHFO temporal activity is explained well by their contemporaneous synchronization-network features. This leads us to the next question that explores potential changes in such correlations on surgical intervention: (2) *Can successful surgery be viewed as a means of sufficiently perturbing the network dynamics, such that the residual network dynamics involving only the preserved regions (i.e. post*

surgery) can no longer sustain, and hence, can no longer predict channel-level epileptiform biomarkers?

To test this hypothesis, we design a two-dimensional feature vector (see Eqn. 11) that captures changes in synchronization dynamics and their correlations with spk-HFO rates when conditioned on a given resection margin. Specifically, we treat surgery as a *network perturbation* tool and quantify how correlations change in the *preserved* tissue after resection. Fig. 2 provides example results from a seizure free (SF) patient (left) and a non-seizure free (NSF) patient (right). In the SF exemplar, residual dynamics of the preserved-only channels fail to adequately predict spkHFO rates (uniformly lower R^2), implying that resection removed key *generator* or synchronization-network-supporting channels. In the NSF exemplar, on the other hand, correlations of the residual dynamics of preserved-only channels with spkHFO rates remianed close to pre-resection values, indicating that synchronization dynamics post-surgery can still generate channel-level epileptoform discharges. This motivates the two-dimensional feature in Eqn. 11 quantifying the network-dynamics disruption due to a candidate surgery. Using this feature *we address the standard validation framework in the field*: predict the post-surgery outcome on a retrospective patient cohort. Our 2-dimensional feature predicts post-surgery outcomes on a retrospective patient cohort of 159 patients with a cross-validated mean $F1$ score of 95%, *significantly outperforming* SOZ resection ($F1 = 78\%$) and spkHFO resection ($F1 = 79\%$) ratio based features.

NetCorr's novelty lies in linking established channel-level and interictal network biomarkers through a regression-based coupling statistic, then using resection-induced coupling changes as a compact patient-level outcome signature.

2 Materials and Methods

2.1 Cohort, recordings, and preprocessing

We analyzed a multi-institutional retrospective cohort of 159 pediatric-onset ($\leq$21 years) focal DRE patients who underwent invasive iEEG monitoring followed by resective surgery (Open iEEG dataset [23]). Inclusion required (i) subdural and/or depth/SEEG iEEG with sampling rate $\geq$1,000 Hz, (ii) an artifact-free slow-wave sleep epoch of $\geq$5 min at least 2 h from seizures, and (iii) post-operative outcome at $\geq$12 months; cases without reliable electrode localization or outcome data were excluded. Outcomes were binarized using ILAE criteria (class I: SF, $n = 113$; classes II–VI: NSF, $n = 46$) [20]. Signals were bipolar referenced, notch filtered for line noise and harmonics, and artifact-free interictal epochs (typically 5–90 min) from the first night (prior to medication tapering) were used for analysis. To account for variable recording duration, coupling was estimated within each patient from 1-s windows and summarized using preserved-channel distributional statistics rather than raw spk-HFO counts.

2.2 spk-HFO detection using expert guided deep learning model

We detected spkHFO events using `pyHFO 2.0`, an open-source deep-learning-based analysis platform that includes built-in preprocessing utilities for denoising and artifact mitigation [4]. In `pyHFO 2.0`, the detection models are fine-tuned using expert annotations with iterative clinician feedback, yielding a reliable spkHFO detector for clinical iEEG.

2.3 Ripple-band interictal synchronization networks

We constructed time-varying directed, weighted synchronization networks in 1-second non-overlapping windows using ripple-band (80–250 Hz) activity [17]. For each window, nodes correspond to iEEG channels and edge weights quantify band-limited coupling. Let $P_{i,m}$ and $\phi_{i,m}$ be the magnitude and phase at ripple-band frequency bin m ($m = 1, \ldots, K$) for channel i. We define an antisymmetric phase-coupling term

$$\sigma_{ij}^{\phi} = -\sigma_{ji}^{\phi} = \frac{1}{K} \sum_{m=1}^{K} \sin(\phi_{j,m} - \phi_{i,m}), \tag{1}$$

and band-limited power

$$P_i = \sum_{m=1}^{K} |P_{i,m}|^2, \qquad \sigma_{ij}^{P} = P_i + P_j. \tag{2}$$

The synchronization coefficient is

$$d_{ij} = \sigma_{ij}^{P}\, \sigma_{ij}^{\phi}, \tag{3}$$

mapped to a bounded edge weight

$$w_{ij} = 1 - \exp(-|d_{ij}|) \in [0, 1]. \tag{4}$$

Within each window we retain only the top 10% of w_{ij} values (adaptive sparsification) and set all other edges to zero. Adaptive sparsification retained the strongest within-window synchronization edges, controlled graph density across patients and time windows, and reduced weak nonspecific edges. Edge direction is assigned using the ripple-band total phase $\eta_i^{\phi} = \sum_{m=1}^{K} \phi_{i,m}$: if $\eta_j^{\phi} > \eta_i^{\phi}$ we orient $i \to j$, otherwise $j \to i$. This yields a sequence of directed, weighted graphs describing second-by-second interictal synchrony.

2.4 Regression based synchronization network–spkHFO coupling

Interictal synchronization networks and spkHFO activity exhibit strongly non-stationary, burst-like temporal structure. As illustrated in Fig. 1, global network integration (Fiedler eigenvalue) shows intermittent surges consistent with transient synchronization events, and the spkHFO rate exhibits temporally aligned

bursts. Moreover, at the channel level, increases in a node's network importance (eigenvector centrality) coincide with higher spkHFO rate in the same channel. These observations motivate a coupling model that asks whether spkHFO fluctuations can be explained by a channel's contemporaneous participation in the interictal synchronization network.

For each channel c, we quantify how well its time-varying spk-HFO activity is explained by contemporaneous network participation. Let $y_c[k]$ be the number of verified spk-HFOs in the k-th 1 s window. To reduce sparsity and timing jitter, we convert counts to a smooth local rate by gaussian kernel convolution,

$$r_c[k] = (h * y_c)[k] = \sum_{\tau=-L}^{L} h[\tau]\, y_c[k-\tau], \tag{5}$$

[2]. For each window we compute three network features for channel c: fiedler weighted in-degree $\mathrm{in}_c[k]$, fiedler weighted out-degree $\mathrm{out}_c[k]$, and eigenvector centrality $\mathrm{eig}_c[k]$, and apply the same gaussian kernel to obtain $\tilde{\mathrm{in}}_c[k]$, $\tilde{\mathrm{out}}_c[k]$, and $\tilde{\mathrm{eig}}_c[k]$. These features summarize complementary aspects of channel participation: incoming synchronization, outgoing synchronization, and global centrality. We then fit an ordinary least squares model per channel,

$$r_c[k] = \beta_{0,c} + \beta_{1,c}\tilde{\mathrm{in}}_c[k] + \beta_{2,c}\tilde{\mathrm{out}}_c[k] + \beta_{3,c}\tilde{\mathrm{eig}}_c[k] + \epsilon_c[k], \tag{6}$$

and define channel-wise coupling strength by the coefficient of determination,

$$R_c^2 = 1 - \frac{\sum_k (r_c[k] - \hat{r}_c[k])^2}{\sum_k (r_c[k] - \bar{r}_c)^2}. \tag{7}$$

We use a linear model to obtain a stable, interpretable explainability statistic (R_c^2) that is comparable across channels and patients.

2.5 Network perturbation feature for surgical outcome prediction

We model resection as a *network perturbation* and quantify how coupling changes in the *preserved* tissue after removing resected channels from the synchronization network.

Pre- vs. post-resection coupling on preserved channel set. For each patient p, let $\mathcal{P}_p$ denote the set of *preserved* channels. We compute channel-wise coupling scores for each $c \in \mathcal{P}_p$ under two conditions: (i) **Pre-drop (full-network) coupling**, $R^{2,\mathrm{all}}_{p,c}$: computed using the original synchronization network constructed from *all* implanted channels. (ii) **Post-drop (preserved-only) coupling**, $R^{2,\mathrm{pres}}_{p,c}$: recomputed after removing all resected channels, reconstructing the synchronization network on preserved channels only, and refitting the channel-wise regression model on the preserved-channel network features.

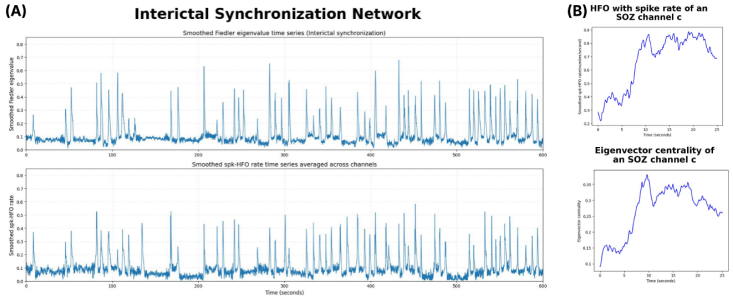

Fig. 1. Interictal network dynamics align with spkHFO activity. (A) The Fiedler eigenvalue exhibits burst-like increases, indicating intermittent episodes of global synchronization; the channel-averaged spkHFO rate shows temporally similar bursts. (B) In a representative SOZ channel, spkHFO rate co-varies with the channel's eigenvector centrality, motivating a coupling model between network participation and pathological event dynamics.

Preserved-channel coupling summaries before and after resection induced perturbation We summarize the preserved-channel coupling distributions using their mean and variance:

$$\mu_p^{\text{all}\to\mathcal{P}} = \frac{1}{|\mathcal{P}_p|}\sum_{c\in\mathcal{P}_p} R_{p,c}^{2,\text{all}}, \qquad v_p^{\text{all}\to\mathcal{P}} = \text{Var}_{c\in\mathcal{P}_p}\left(R_{p,c}^{2,\text{all}}\right), \tag{8}$$

$$\mu_p^{\text{pres}} = \frac{1}{|\mathcal{P}_p|}\sum_{c\in\mathcal{P}_p} R_{p,c}^{2,\text{pres}}, \qquad v_p^{\text{pres}} = \text{Var}_{c\in\mathcal{P}_p}\left(R_{p,c}^{2,\text{pres}}\right). \tag{9}$$

2D perturbation feature vector. We define the patient-level resection-induced perturbation feature vector as the change in preserved-channel mean and variance of coupling:

$$\Delta\mu_p = \mu_p^{\text{all}\to\mathcal{P}} - \mu_p^{\text{pres}}, \qquad \Delta v_p = v_p^{\text{all}\to\mathcal{P}} - v_p^{\text{pres}}, \tag{10}$$

$$\mathbf{x}_p^{\text{pert}} = \begin{bmatrix}\Delta\mu_p \\ \Delta v_p\end{bmatrix}. \tag{11}$$

Outcome prediction and evaluation. We use $\mathbf{x}_p^{\text{pert}}$ as a compact resection-induced patient representation for surgical outcome prediction. We train a k-nearest neighbors (kNN) classifier in this 2D feature space and evaluate performance using stratified 10-fold cross-validation at the patient level. Within each training fold, features are z-scored using training-fold statistics only, and the same transformation is applied to the held-out fold to prevent information leakage. We report out-of-fold predicted probabilities of seizure freedom, aggregated confusion matrix, ROC/AUC, and fold-wise accuracy, precision, recall, and F1 score (mean ± standard deviation across folds).

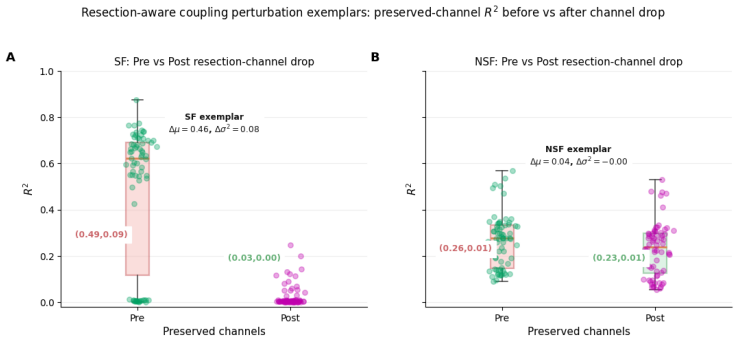

Fig. 2. Resection-induced coupling perturbation exemplars. Preserved-channel network–spkHFO coupling (R^2) is shown before (Pre; full implanted network) and after (Post; resected channels removed and the synchronization network recomputed on preserved channels only) for representative (A) SF and (B) NSF patients. Boxplots summarize preserved-channel distributions; points denote individual channels.

3 Results

3.1 Network perturbation produces outcome-specific shifts in preserved-channel coupling

At the cohort level, resection-induced perturbation produces outcome-specific shifts in preserved-channel network–spkHFO coupling. Fig. 3A summarizes each patient by $(\Delta\mu_p, \Delta v_p)$, the change in the mean and variance of preserved-channel coupling (R^2) after removing resected channels and recomputing coupling on preserved tissue. SF patients cluster in a region characterized by larger coupling disruption (higher $\Delta\mu_p$ with systematic shifts in Δv_p), whereas NSF patients concentrate near smaller perturbation effects (lower $\Delta\mu_p$), indicating that network-explainable pathological activity persists in preserved tissue. The separation of group centroids in this space further highlights that the resection perturbation induces distinct, population-level coupling responses in SF versus NSF patients.

3.2 Patient-level network perturbation features predict postoperative outcome

The outcome-specific structure observed in Fig. 3A suggests that resection-induced perturbations of preserved-channel coupling can be leveraged directly for outcome prediction. Using these patient-level perturbation features ($\Delta\mu_p$,Δv_p), a kNN classifier yields well-separated out-of-fold seizure-freedom probabilities (Fig. 3B) with robust cross-validated performance, as reflected by the aggregated confusion matrix and high ROC AUC (Fig. 3C–D). Compared with spkHFO- and SOZ- resection ratio based baselines, *NetCorr* achieves the strongest performance across accuracy, precision, recall, and F1 (mean $F1 = 0.95$; Fig. 3E).

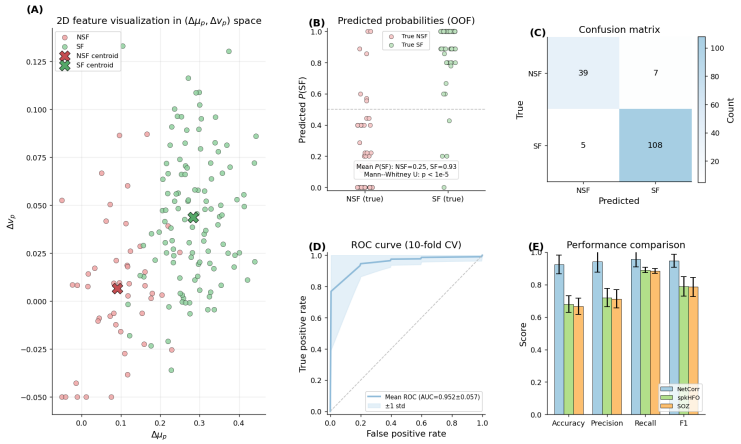

Fig. 3. Network perturbation feature visualization and postoperative outcome prediction. (A) Patient-level feature distribution in the network perturbation feature space ($\Delta\mu_p$,Δv_p). SF and NSF patients occupy separable regions in this space. (B) Out-of-fold kNN-predicted probability of seizure freedom, stratified by true outcome (NSF vs. SF), showing significant separation between groups (Mann–Whitney U test). (C) Aggregated confusion matrix across stratified 10-fold cross-validation. (D) Mean ROC curve across folds with ±1 standard deviation band (AUC reported in legend). (E) Performance comparison (mean ± standard deviation across folds) of *NetCorr* against spkHFO- and SOZ-based baselines for accuracy, precision, recall, and F1 score. *NetCorr* (mean F1 score - 95%) significantly outperforms the spkHFO-based model (mean F1 score - 79%) and SOZ resection status-based model (mean F1 score - 78%) on all four performance metrics.

Together, these results show that resection-induced changes in preserved-tissue coupling provide an accurate interictal predictor of surgical outcome and motivate their use as a quantitative measure of resection sufficiency.

4 Discussion and concluding remarks

There are several translational implications of the *NetCorr* framework beyond its use in accurately predicting post-surgery seizure freedom. First, *NetCorr* embeds an intervention perspective and can be translated into surgery planning. By treating surgery as a network perturbation and quantifying the residual coupling in preserved channels, the framework moves from static localization toward an actionable question: how much pathological network organization is expected to remain after removing a candidate set of channels? This creates a natural foundation for future in-silico resection-margin tools, where alternative margins (or electrode coverage strategies) could be compared by their predicted impact on network-explainable pathology before definitive surgery.

Second, iEEG provides only partial coverage of the epileptogenic network, so postoperative failure can arise from under-sampling, as well as, suboptimal

resection [14, 16, 10]. Persistently low preserved-channel coupling before and after resection is consistent with dominant generators lying outside the sampled network. In our cohort, we observe a distinct NSF subgroup of $n = 14$ patients with near-floor coupling that changes minimally after resection (mean preserved-channel $R^2 = 0.09$ pre-surgery versus 0.08 post-surgery), therefore providing a quantitative signature of potential unsampled epileptogenic regions.

Limitations and future work. Network–spkHFO coupling may depend on sleep stage, medication level, and seizure proximity, motivating future state-aware analyses. The perturbation signature may also be sensitive to artifact selection, residual noise, spkHFO detection, smoothing, network construction, and sparsification; future work should evaluate robustness to these factors and to shorter recordings. Although NetCorr outperformed SOZ- and spkHFO-resection ratio baselines, future studies should compare against stronger single-modality HFO-only [22] and network-only [13] baselines on the same iEEG corpus. Broader stratified validation across institutions, implant types, etiologies, age groups, pathologies, and outcome subtypes is needed to establish generalizability.

Disclosure of Interests

The authors have no competing interests to declare that are relevant to the content of this article.

References

1. Bassett, D.S., Sporns, O.: Network neuroscience. Nature Neuroscience **20**(3), 353–364 (2017). https://doi.org/10.1038/nn.4502
2. Cunningham, J.P., Gilja, V., Ryu, S.I., Shenoy, K.V.: Methods for estimating neural firing rates, and their application to brain–machine interfaces. Neural Networks **22**(9), 1235–1246 (2009). https://doi.org/10.1016/j.neunet.2009.02.004
3. Devinsky, O., Hesdorffer, D.C., Thurman, D.J., Lhatoo, S., Richerson, G.: Sudden unexpected death in epilepsy: epidemiology, mechanisms, and prevention. The Lancet Neurology **15**(10), 1075–1088 (2016). https://doi.org/10.1016/S1474-4422(16)30158-2
4. Ding, Y., Zhang, Y., Duan, C., Daida, A., Zhang, Y., Kanai, S., Lu, M., Hussain, S., Staba, R.J., Nariai, H., Roychowdhury, V.: Pyhfo 2.0: an open-source platform for deep learning-based clinical high-frequency oscillations analysis. Journal of Neural Engineering **22**(5), 056040 (2025). https://doi.org/10.1088/1741-2552/ae10e0
5. Engel, J.J.: Why is there still doubt to cut it out? Epilepsy Currents **13**(5), 198–204 (2013). https://doi.org/10.5698/1535-7597-13.5.198
6. Engel, J.J., McDermott, M.P., Wiebe, S., Langfitt, J.T., Stern, J.M., Dewar, S., Sperling, M.R., Gardiner, I., Erba, G., Fried, I., Jacobs, M., Vinters, H.V., Mintzer, S., Kanner, A., Silbergeld, D.L., Dunn, D., Bartolucci, A.: Early surgical therapy for drug-resistant temporal lobe epilepsy: A randomized trial. JAMA **307**(9), 922–930 (2012). https://doi.org/10.1001/jama.2012.220
7. Fisher, R.S., Acevedo, C., Arzimanoglou, A., Bogacz, A., Cross, J.H., Elger, C.E., Engel, J.J., Forsgren, L., French, J.A., Glynn, M., Hesdorffer, D.C., Lee, B.I.,

Mathern, G.W., Moshe, S.L., Perucca, E., Scheffer, I.E., Tomson, T., Watanabe, M., Wiebe, S.: Ilae official report: A practical clinical definition of epilepsy. Epilepsia **55**(4), 475–482 (2014). https://doi.org/10.1111/epi.12550

8. Gunnarsdottir, K.M., Li, A., Smith, R.J., Kang, J.Y., Korzeniewska, A., Crone, N.E., Rouse, A.G., Cheng, J.J., Kinsman, M.J., Landazuri, P., Uysal, U., Ulloa, C.M., Cameron, N., Cajigas, I., Jagid, J., Kanner, A., Elarjani, T., Melo Bicchi, M., Inati, S., Zaghloul, K.A., Boerwinkle, V.L., Wyckoff, S., Barot, N., Gonzalez-Martinez, J., Sarma, S.V.: Source-sink connectivity: a novel interictal eeg marker for seizure localization. Brain **145**(11), 3901–3915 (2022). https://doi.org/10.1093/brain/awac300
9. Jacobs, J., Zijlmans, M., Zelmann, R., Chatillon, C.É., Hall, J., Olivier, A., Dubeau, F., Gotman, J.: High-frequency electroencephalographic oscillations correlate with outcome of epilepsy surgery. Annals of Neurology **67**(2), 209–220 (2010). https://doi.org/10.1002/ana.21847
10. Jehi, L., Yardi, R., Chagin, K., Tassi, L., Russo, G.L., Worrell, G., Hu, W., Cendes, F., Morita, M., Bartolomei, F., et al.: Development and validation of nomograms to provide individualised predictions of seizure outcomes after epilepsy surgery: a retrospective analysis. The Lancet Neurology **14**(3), 283–290 (2015). https://doi.org/10.1016/S1474-4422(14)70325-4
11. Kwan, P., Arzimanoglou, A., Berg, A.T., Brodie, M.J., Hauser, W.A., Mathern, G., Moshe, S.L., Perucca, E., Wiebe, S., French, J.: Definition of drug resistant epilepsy: Consensus proposal by the ad hoc task force of the ilae commission on therapeutic strategies. Epilepsia **51**(6), 1069–1077 (2010). https://doi.org/10.1111/j.1528-1167.2009.02397.x
12. Li, A., Huynh, C., Fitzgerald, Z., et al.: Neural fragility as an eeg marker of the seizure onset zone. Nature Neuroscience **24**(10), 1465–1474 (2021). https://doi.org/10.1038/s41593-021-00901-w
13. Monsoor, T., Kanai, S., Daida, A., Kuroda, N., Sinha, P., Oana, S., Zhang, Y., Liu, L., Singh, G., Duan, C., et al.: Mini-seizures: Novel interictal ieeg biomarker capturing synchronization network dynamics at the epileptogenic zone. medRxiv (2025). https://doi.org/10.1101/2025.01.31.25321482
14. Rosenow, F., Luders, H.: Presurgical evaluation of epilepsy. Brain **124**(9), 1683–1700 (2001). https://doi.org/10.1093/brain/124.9.1683
15. Shi, W., Shaw, D., Walsh, K.G., Han, X., Eden, U.T., Richardson, R.M., Gliske, S.V., Jacobs, J., Brinkmann, B.H., Worrell, G.A., Stacey, W.C., Frauscher, B., Thomas, J., Kramer, M.A., Chu, C.J.: Spike ripples localize the epileptogenic zone best: an international intracranial study. Brain **147**(7), 2496–2506 (2024). https://doi.org/10.1093/brain/awae037
16. Spencer, S.S.: Neural networks in human epilepsy: evidence of and implications for treatment. Epilepsia **43**(3), 219–227 (2002). https://doi.org/10.1046/j.1528-1157.2002.26901.x
17. Wang, S., Herzog, E.D., Kiss, I.Z., Schwartz, W.J., Bloch, G., Sebek, M., Granados-Fuentes, D., Wang, L., Li, J.S.: Inferring dynamic topology for decoding spatiotemporal structures in complex heterogeneous networks. Proceedings of the National Academy of Sciences of the United States of America **115**(37), 9300–9305 (2018). https://doi.org/10.1073/pnas.1721286115
18. Weiss, S.A., Waldman, Z., Raimondo, F., Slezak, D., Donmez, M., Worrell, G., Bragin, A., Engel, J., Staba, R., Sperling, M.: Localizing epileptogenic regions using high-frequency oscillations and machine learning. Biomarkers in Medicine **13**(5), 409–418 (2019). https://doi.org/10.2217/bmm-2018-0335

19. Wiebe, S., Blume, W.T., Girvin, J.P., Eliasziw, M.: A randomized, controlled trial of surgery for temporal-lobe epilepsy. The New England Journal of Medicine **345**(5), 311–318 (2001). https://doi.org/10.1056/NEJM200108023450501
20. Wieser, H., Blume, W., Fish, D., Goldensohn, E., Hufnagel, A., King, D., Sperling, M., Luders, H.: Proposal for a new classification of outcome with respect to epileptic seizures following epilepsy surgery. Epilepsia (Series 4) **42**(2) (2001). https://doi.org/10.1046/j.1528-1157.2001.4220282.x
21. World Health Organization: Epilepsy (fact sheet). Website (2024), https://www.who.int/news-room/fact-sheets/detail/epilepsy, accessed 2026-02-03
22. Zhang, Y., Daida, A., Liu, L., Kuroda, N., Ding, Y., Oana, S., Kanai, S., Monsoor, T., Duan, C., Hussain, S.A., Qiao, J.X., Salamon, N., Fallah, A., Sim, M.S., Sankar, R., Staba, R.J., Engel, J., Asano, E., Roychowdhury, V., Nariai, H.: Self-supervised data-driven approach defines pathological high-frequency oscillations in epilepsy. Epilepsia (2025). https://doi.org/10.1111/epi.18545
23. Zhang, Y., Daida, A., Liu, L., Kuroda, N., Ding, Y., Oana, S., Monsoor, T., Duan, C., Hussain, S.A., Qiao, J.X., Salamon, N., Fallah, A., Sim, M.S., Sankar, R., Staba, R.J., Jr., J.E., Asano, E., Roychowdhury, V., Nariai, H.: "open ieeg dataset" (2024). https://doi.org/doi:10.18112/openneuro.ds005398.v1.0.1
24. Zhang, Y., Lu, Q., Monsoor, T., Hussain, S.A., Qiao, J.X., Salamon, N., Fallah, A., Sim, M.S., Asano, E., Sankar, R., Staba, R.J., Engel, J., Speier, W., Roychowdhury, V., Nariai, H.: Refining epileptogenic high-frequency oscillations using deep learning: a reverse engineering approach. Brain Communications **4**(1), fcab267 (2022). https://doi.org/10.1093/braincomms/fcab267